ADVANCED ENERGY MATERIALS
www.advenergymat.de

Going Beyond Lithium Hybrid Capacitors: Proposing a New High-Performing Sodium Hybrid Capacitor System for Next-Generation Hybrid Vehicles Made with Bio-Inspired Activated Carbon

*Ranjith Thangavel, Karthikeyan Kaliyappan, Kisuk Kang, Xueliang Sun, and Yun-Sung Lee**

A novel sodium hybrid capacitor (NHC) is constructed with an intercalation-type sodium material [carbon coated-$Na_3V_2(PO_4)_3$, C-NVP] and high surface area-activated carbon derived from an eco-friendly resource cinnamon sticks (CDCs) in an organic electrolyte. This novel NHC possesses a combination of high energy and high power density, along with remarkable electrochemical stability. In addition, the C-NVP/CDC system outperforms present, well-established lithium hybrid capacitor systems in all areas, and can thus be added to the list of candidates for future electric vehicles. A careful optimization of mass balance between electrode materials enables the C-NVP/CDC cell to exhibit extraordinary capacitance performance. This novel NHC produces an energy density of 118 Wh kg^{-1} at a specific power of 95 W kg^{-1} and retains an energy density of 60 Wh kg^{-1} with high specific power of 850 W kg^{-1}. Furthermore, a discharge capacitance of 53 F g^{-1} is obtained from the C-NVP/CDC cell at a 1 mA cm^{-2} current density, along with 95% capacitance retention, even after 10 000 cycles. The sluggish kinetics of the Na ion battery system is successfully overcome by developing a stable, high-performing NHC system.

1. Introduction

The trend of research among researchers around the world in energy storage devices is turning toward sodium ion-based systems.[1,2] Such systems are a prime candidate for next-generation hybrid electric vehicles (HEVs) and plugin hybrid electric vehicles (PHEVs),[3–5] as a replacement for Li-ion energy storage systems, for which there is much less interest despite their high energy density.[6–8] This is mainly because of the increase in both demand and the price of lithium resources. Lithium availability is low, which significantly affects the commercialization of Li-ion storage systems for power grids and HEVs.[9–11] Although, lithium recycling could provide a possible solution, it is still in the early stages of the research and has a long way to go.[3,12] Looking for other possible solutions, sodium ion-based energy storage systems could be an alternative because sodium is widely available and inexpensive; it even has a suitable redox potential ($E_{o\ (Na^+/Na)}$ = –2.71 V vs SHE, Standard Hydrogen Electrode).[10,13–15] A wide range of electrode materials such as $NaFe_{0.5}Mn_{0.5}O_2$,[16] Na_xCoO_2,[17] $Na[Ni_{0.25}Fe_{0.5}Mn_{0.25}]O_2$,[18] $Na_3V_2(PO_4)_3$,[19,20] Na_xVO_2,[21] and $Na_3V_2(PO_4)_2F_3$[22] have been extensively studied for sodium ion battery application. However, the sluggish kinetics of sodium ion electrode materials due to the larger ionic radii of sodium ions (0.98 Å) severely affects the performance of the system.[23–25] It is thus essential to develop stable energy sources for sodium-based energy storage systems.

In this regard, sodium-ion hybrid capacitors (NHCs) can be constructed to achieve the desired performance, in which high-energy density along with enhanced power density could be obtained. Generally, hybrid capacitors have a combination of nonfaradaic (carbonaceous materials) and faradaic (metal oxides or intercalation materials) electrodes in an aqueous/nonaqueous electrolyte. The NHC stores charge by surface adsorption and desorption over the nonfaradaic material and by sodium intercalation/deintercalation on the faradaic material. This combined effect results in high power density and energy density simultaneously, along with good cyclability when used in an organic electrolyte, as it has a wide operating potential window.[26–29] The choice of electrode material is the most essential part in developing a stable high-performance NHC. Rather than focusing on the mass balance between the electrodes, the kinetics of the two electrodes must be in balance to fabricate a stable and efficient NHC system.[30] The faradaic electrode

R. Thangavel, Prof. Y.-S. Lee
Faculty of Applied Chemical Engineering
Chonnam National University
Gwang-ju 500-757, South Korea
E-mail: leeys@chonnam.ac.kr
Dr. K. Kaliyappan, Prof. X. Sun
Department of Mechanical and Materials Engineering
University of Western Ontario
Ontario, London N6A 5B9, Canada
Prof. K. Kang
Department of Materials Science and Engineering
Seoul National University
Seoul 151-742, South Korea

DOI: 10.1002/aenm.201502199

materials that work on the intercalation process always exhibit slower ionic diffusion and sluggish reaction kinetics. By using an intercalation compound with a high ionic diffusion coefficient, a high-power and highly stable NHC could easily be obtained.[30,31]

Sodium superionic conductor (NASICON)- $Na_3V_2(PO_4)_3$ (NVP) is of great interest because of its (i) high chemical diffusion coefficient, which facilitates faster migration of Na^+ ions between the electrode and the electrolyte (faster than its Li analogue),[20,32] and (ii) high structural and thermal stability as compared to other sodium-based layered intercalation-type electrode materials.[19,33,34] The crystal structure consists of anions of a $(V_2(PO_4)_3)^{3-}$ framework formed by corner-linked $[VO_6]$ octahedral and $[PO_4]$ tetrahedral units. [34] Open, 3D tunnel-like pathways are formed when Na ions occupy two different oxygen interstitial sites.[19,25,35] This facilitates the rapid and facile movement of Na^+ ions through the structure.[36] $Na_3V_2(PO_4)_3$can deliver a capacity of around 120 mA h g^{-1} between 2.5 and 3.8 V when 2 mol of Na^+ insertion/extraction take place. The extraction takes place due to V^{3+} to V^{4+} redox with a 3.3 V flat operating voltage.[20,34,35] However, poor electronic conductivity between the particles diminishes the performance through severe capacity decay and failure at higher current cycling processes.[20,34,36] The performance of the $Na_3V_2(PO_4)_3$ could be improved by developing conductive carbon coating,[20] making composite with graphene,[34] CNT,[37] and cation substitutions in both Na and V sites as well.[38,39] Conductive carbon coating can improve the reaction kinetics by offering faster electronic and ionic pathways for both electrons and sodium ions. [40]

On the other hand, highly porous activated carbon has been extensively studied as nonfaradaic electrode material for hybrid capacitors because of their high electrical conductivity, high surface area, and high thermal and chemical stability, along with low cost.[41,42] Conventional activated carbon (AC) from coal, petroleum coke, and needle coke is generally used.[42] However, in addition to the difficulty with the physical activation process, high-temperature pyrolysis, the low availability of these fossil fuels, increased energy demand, and environmental issues, which limits its practical usage, even though they have high surface area and high capacitance. The possible solution is AC that can be prepared from eco-friendly bio-inspired resources.[42] In recent days, biomass-derived activated carbon with properties similar to those of conventional AC has been used in electrical double layer capacitors capacitors (EDLCs).[43] Although the carbon yield from these sources is somewhat lower than that from fossil fuel-derived carbon, bio-derived carbon is superior in terms of low cost and wide availability. AC from various biomass sources such as pine cones, coconut shells, bamboo, banana fiber, corn grains, rice husk, sea weed, and recycled waste paper have been synthesized and studied for wide range of applications.[42,43] Research on AC from bioresources has established that highly porous 3D carbon with suitable pore distribution and excellent capacitance properties can be easily prepared, resulting in analogues to conventional AC. To overcome the above mentioned issues, we first synthesized and utilized highly porous carbon derived from cinnamon sticks (CDCs), a commonly used food, as an adsorption/desorption electrode for the NHC. Charcoal obtained by carbonization of the cinnamon sticks was physically activated by treating it with KOH. The obtained CDC possessed a high surface area, along with high electrical conductivity, and thus it facilitated a quick ion adsorption and desorption process, easily forming double layers.

Recently, Jian et al. reported the utilization of an NVP/carbon composite as a high-power electrode for fabricating a symmetric pseudocapacitor.[44] However, the energy density and stability obtained were not sufficient to adopt NVP/carbon composite electrodes in high-energy storage applications. It is essential to develop an electrode material capable of delivering enhanced electrochemical behavior by increasing its active reaction sites. In this work, we evaluated the performance of an NHC constructed with high-surface area NASICON-type carbon-coated $Na_3V_2(PO_4)_3$ (C-NVP) and highly porous carbon derived from natural resources. This novel asymmetric hybrid capacitor exhibited extraordinary cyclic stability, with high power and energy density, providing a good solution to the present issues. The results are discussed in detail.

2. Characterization

2.1. Physical Characterization

X-ray diffraction (XRD) patterns of C-NVP and CDC powders were recorded by Rigaku Rint 1000, Japan with Cu Kα radiation source. N_2 adsorption/desorption isotherms were recorded using a Micromeritics ASAP 2010 surface area analyzer to measure the Brunauer–Emmett–Teller (BET) surface area. The surface and structural morphology of both samples were studied using a scanning electron microscope (FE-SEM, S4700, Hitachi, Japan) and transmission electron microscope (TEM, TECNAI, Philips, Netherlands 200 k eV). X-ray photoelectron spectroscopy (XPS) analyses were performed using a Multilab instrument (monochromatic Al Kα radiation $h\gamma$ = 1486.6 eV). A Raman dispersive spectrometer (Lab Ram HR 800, Horiba, Japan) was used to obtain the laser Raman spectrum for both samples.

2.2. Electrochemical Characterization

The half-cell performance of C-NVP and CDC was measured using either C-NVP or CDC as the working electrode and metallic sodium foil as the counter electrode. The composition of the electrodes was as follows: 80% active material, 10% conductive additive (Ketjenblack), and 10% binder (teflonized acetylene black). The slurry was pressed over a stainless steel mesh and dried at 160 °C for 4 h in vacuum and analyzed in a standard CR 2032 coin-cell configuration. The two electrodes were separated by a porous polypropylene (Celgard 3401, USA) film and filled with 1 M $NaClO_4$ in ethylene carbonate/dimethyl carbonate (1:1 Vol). The NHC was constructed with C-NVP and CDC electrodes after making a proper mass balance between the electrodes. Cyclic voltammetry (CV) and electrochemical impedance spectroscopy results of both the half-cell and the NHC were analyzed with a Bio-Logic electrochemical work station (SP-150), France. A Won-A-Tech Battery tester (WBCS

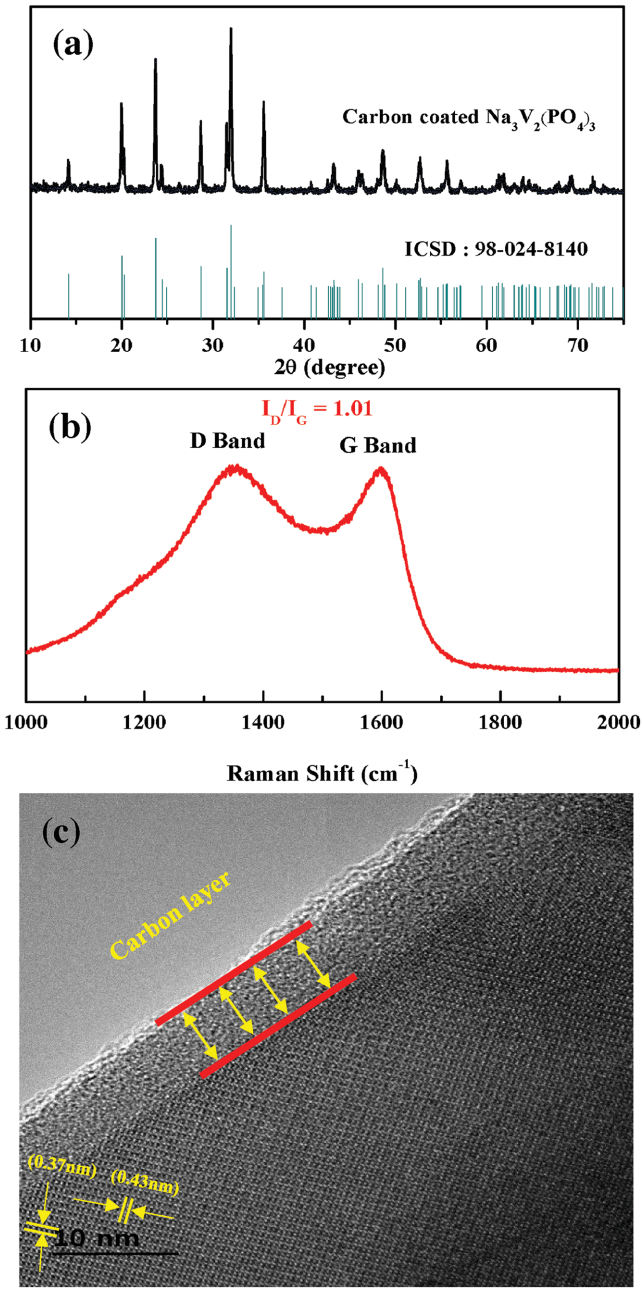

Figure 1. a) XRD pattern of C-NVP, b) Raman spectrum of C-NVP, and c) HR-TEM image of C-NVP.

3000, Korea) was used for galvanostatic charge–discharge studies, which were carried out between 0 and 3 V at different current densities under ambient conditions.

3. Results and Discussion

The XRD patterns of the carbon-coated NVP are presented in **Figure 1**a. The synthesized NVP particles had a hexagonal crystal structure and were indexed to the *R3C* space group.[45] No impurities due to V_2O_5 or Na_3PO_4 were detected. The results are consistent with reference pattern ICSD: 98-024-8140.[45] The Raman spectrum for the carbon-coated NVP is presented in Figure 1b. It exhibited typical characteristic peaks at ≈1350 cm^{-1} (D band, corresponding to symmetric E2g vibration of graphite-like materials) and ≈1590 cm^{-1} (G band, which is mainly disordered carbon), which confirms the presence of a carbon layer over the particle. The intensity ratio of the D and G bands (I_D/I_G) was found to be 1.01, which implies that the carbon coating is fairly ordered, increasing the electronic conductivity between adjacent NVP particles.[46,45]

The pore size and surface area of the carbon-coated NVP particles were investigated using the nitrogen isotherm adsorption technique (Figure SS 1a, Supporting Information). The presence of the hysteresis loop indicates a type-IV isotherm and the presence of mesopores. This mesoporous structure had a high surface area of ≈45 m^2 g^{-1}, which is higher than other reported values.[33,34,39,40] The average Barrett–Joiner–Halenda (BJH) pore diameter of the particles was found to be 12 nm (Figure SS 1b, Supporting Information). Both the mesoporous structure and smaller size of the particles were retained even after high-temperature calcination. The reduced size of the electroactive material provided improved ionic transport for the sodium ions. The presence of mesopores is crucial for the superior electrochemical performance of any material. The C-NVP has a high effective surface area that acts as a reaction site for sodium ion penetration.[40,47] This easily allows the sodium ions to diffuse easily and quickly into the particles by taking a shorter path.[47] Thus, enhanced electrochemical behavior is expected from C-NVP, even at high current, as the larger surface area allows all of the active material to contribute in the reaction.

The morphology of C-NVP is analyzed by SEM and corresponding image is shown in Figure SS2 in the Supporting Information. The SEM confirmed that the particles were almost spherical in shape, with an average size of 2 µm, and that they were well connected, along with a large number of mesopores. The HR-TEM (Figure 1c) image confirms the presence of a very uniform carbon nanolayer over the NVP surface, which provides sufficient electronic conductivity between the particles. Further the lattice fringes are clearly visible in the image, indicating that the NVP particles are highly crystalline in nature. The lattice fringes have the *d*-spacings of around 0.37 and 0.43 nm which corresponds to (113) and (110) lattice planes of NASICON-type NVP, respectively. The carbon nanolayer (≈5 nm) covered the particle surfaces uniformly and bridged all the particles. This arrangement enhanced the electronic conductivity, enabling the electrons to access the NVP particles quickly, facilitating good performance at higher current. The amount of carbon in C-NVP is found to be ≈2 wt% by thermogravimetric analysis (TGA). The weight loss between 300 and 400 °C is the measure of amount of carbon of present in C-NVP (Figure SS 3, Supporting Information). The carbon-bridged NVP particles can exhibit superior capacitive activity with longer cyclic stability.[20,40]

The XPS spectrum of C-NVP in Figure SS 4a in the Supporting Information confirms the presence of Na, V, P, and O, along with carbon, which indicates that the particles are well covered by carbon. The $V2_p$ spectrum (Figure SS 4b, Supporting Information) was analyzed to confirm the oxidation state of vanadium in C-NVP. The peaks at binding energy values of

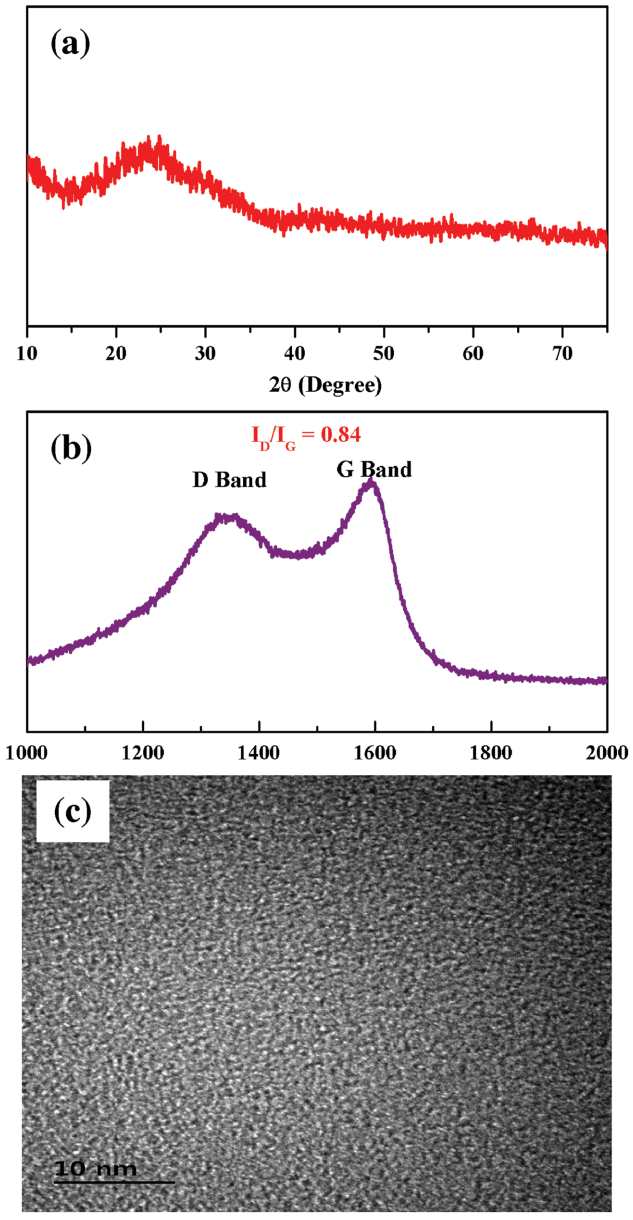

Figure 2. a) XRD pattern of CDC, b) Raman spectrum of CDC, and c) TEM image of CDC.

≈517 eV and ≈524 eV correspond to V $2p_{3/2}$ and V $2p_{1/2}$, respectively, confirming that vanadium is in a trivalent state.[48] Further peaks due to C1s core levels are also seen, along with surface functional groups such as –OH and –COOH.[49]

The XRD pattern of CDC in **Figure 2**a clearly confirms the amorphous nature of the carbon. Two peaks are visible, a broad peak at 2θ between 20° and 30° and a peak at 2θ of 43°, which correspond to the (002) and (001) planes, respectively. The broad first peak indicates the disordered graphitic form of the amorphous carbon; second peak indicates that the carbon is highly turbostratic in nature after activation with KOH.[50] The morphology of CDC was analyzed by TEM and SEM, and the results are presented in Figure 2c and Figure SS 5 (Supporting Information), respectively. The image shows the presence of a 3D, hierarchically oriented combination of micro and mesopores. These pores are highly interconnected, which is the reason for their high surface area that easily accommodates larger numbers of ions over their surface. The obtained BET surface was 1540 $m^2\ g^{-1}$, making it a suitable material for hybrid capacitors. The electrolyte can easily penetrate this morphology, and the number of active sites for charge storage is greatly increased. This clearly shows that CDC could be applied in both EDLCs and hybrid capacitors.[41,42] The nitrogen isotherm adsorption isotherm presented in Figure SS 6a in the Supporting Information exhibits a type II isotherm, which means CDC has a combination of micro, meso, and macropores. The BJH pore size distribution (Figure SS 6b, Supporting Information) showed a large number of mesopores in CDC, in which a large number of Na^+ ions could be arranged. Also, the presence of a small number of macropores favors adsorption by acting as an electrolyte reservoir. Further analysis of CDC was done by Raman spectroscopy, and the results are shown in Figure 2b. The D and G bands of carbon show their graphitic nature characteristic vibrations at ≈1350 and ≈1595 cm^{-1}, respectively. The G-band results from symmetric E2g vibrations mode of graphite-like materials whereas the D-band corresponds to the breathing mode of k-point phonons of A1g symmetry.[51] The I_D/I_G ratio for CDC was calculated to be 0.84 indicating the presence of defects especially the pores and surface functionalities formed. It is well known that the prominent peak ≈1595 cm^{-1} is attributed to disordered sp^3 bonded graphitic carbon, enabling the enhancement of ionic/electronic transfer of CDC material and hence outstanding improvement in electrochemical performance can be achieved. [51] XPS analysis was used to analyze the surface features of CDC and core-level C1s and O1s, and the results are presented in Figure SS 7a and b in the Supporting Information, respectively. In the C1s spectra, the peak around 284.6 eV arose due to the binding energy of sp^2 C–C. Functional groups such as carboxyl and hydroxyl groups were also confirmed, with characteristic peaks around binding energies of 288.5 and 286 eV, respectively.[52,49] The functional groups over carbon in both C-NVP and CDC can easily wet the surface and facilitate adsorption process over the surface, which helps in forming a double layer.

3.1. Half-Cell Performance

The sodium ion storage performance of C-NVP and CDC against sodium foil in a half-cell configuration was initially analyzed before constructing the NHC. **Figure 3**a shows the sodium ion storage performance of C-NVP in cathodic region between 2.5 and 3.8 V versus Na^+/Na at a 0.25 C rate. The performance shows a plateau at approximately 3.4 V, which is due to the reversible phase transformation between $NaV_2(PO_4)_3$ and $Na_3V_2(PO_4)_3$ because of the V^{3+}/V^{4+} redox reaction.[34,35,47] It delivers an initial discharge capacity of 110 mA h g^{-1} at 0.25 C, and it retains good capacity even after 100 cycles, with a Columbic efficiency of 97%, which is shown in Figure 3b. Further, the C-NVP exhibited a superior rate performance (Figure SS 8a, Supporting Information) by delivering the specific discharge capacity of 110, 104, 100, 96, 94 mA h g^{-1} at 0.5, 1, 1.25, 3, 5 C, respectively. This highly stable nature of

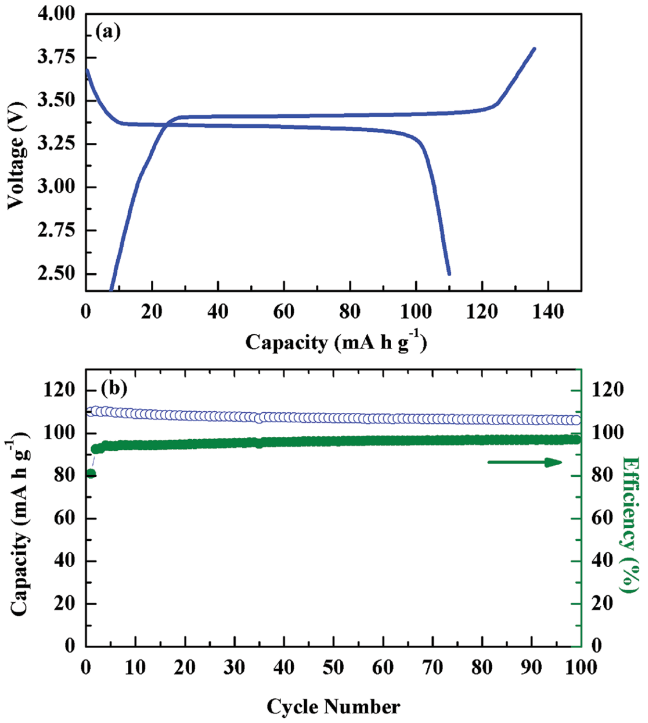

Figure 3. a) Cathodic performance and b) cyclic stability of C-NVP.

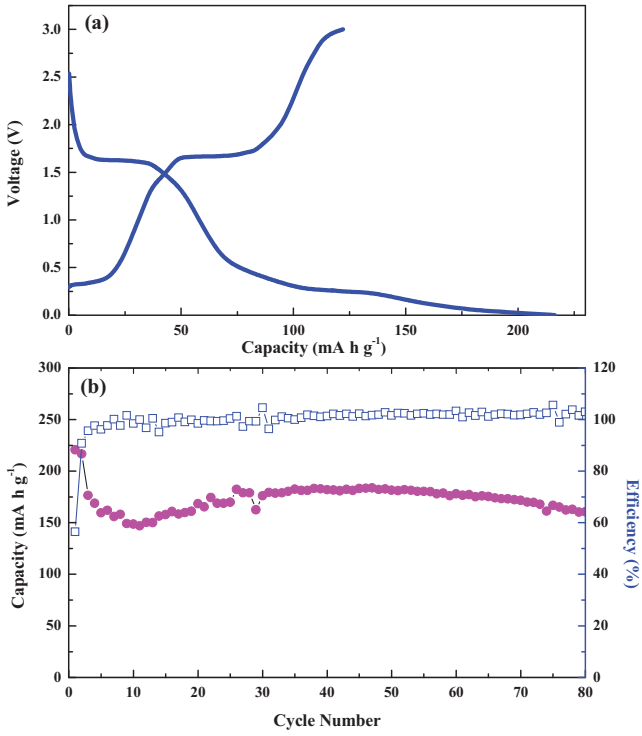

Figure 4. a) Anodic performance and b) cyclic stability of C-NVP.

C-NVP implies that Na^+ ion intercalation/deintercalation is highly reversible and there is no deterioration in their structure. The uniform carbon coating and mesoporosity of C-NVP facilitates easy ionic and electron movement during the charge/discharge process even at high current rate.[40] Similarly, the anodic performance of C-NVP was tested between 3 and 0 V versus Na^+/Na at 25 mA g^{-1} current density (**Figure 4**a). Two plateaus at ≈1.6 and 0.25 V were observed, which are due to the redox reaction of vanadium from V^{3+} to V^{1+}.[53,54] There is 2 Na^+ ion intercalation and deintercalation, which is highly reversible, and thus the phase transformation is between $Na_5V_2(PO_4)_3$ and $Na_3V_2(PO_4)_3$.[54] The discharge capacity of 181 mA h g^{-1} after 50 cycles and 161 mA h g^{-1} after 75 cycles was maintained at 25 mA g^{-1} current density (Figure 4b). Although a low Columbic efficiency was obtained during the initial cycle, it has reached more than 100% in next few cycles and it is maintained throughout. The excess capacity obtained is from the solid-electrolyte interfacial and carbon-coating layers.[53,54] The behavior of C-NVP with different current density in anodic region is evaluated by rate performance studies and presented in Figure SS 8b in the Supporting Information. Superior discharge capacity of 159, 148, 138, 117, 103 mA h g^{-1} is obtained at 0.25, 0.5, 1, 2.5, 5 C, respectively. The results prove the bifunctional property of the C-NVP which can work in both anodic and cathodic region. Further, we have analyzed the phase change in C-NVP electrodes after long-term cycling in both anodic and cathodic region through ex situ XRD technique and the results are presented in Figure SS 9 in the Supporting Information. The XRD patterns of both electrodes has no new peaks, resembling with pristine C-NVP and the only change observed is decrease in intensity of few peaks, indicating that the NASICON structure and crystallinity is still maintained even after long cycling. This depicts the robust nature of NASICON-type C-NVP and making it an attractive and suitable candidate for sodium hybrid capacitor application.

The performance of CDC was tested between 3 and 4.6 V versus Na^+/Na at 400 mA g^{-1}, and the results are presented in **Figure 5**. The linear charge/discharge profile proves that charge storage occurs mainly on the CDC surface and by a surface adsorption/desorption process.[55] An average discharge capacity of 60 mA h g^{-1} was obtained at a current rate of 400 mA g^{-1} and the capacity do not change much with cycling proving the adsorption/desorption process is highly reversible.

3.2. C-NVP/CDC Hybrid Capacitor

A proper mass balance between the C-NVP and CDC electrodes was carried out while constructing the full cell to attain a highly efficient NHC. Based on the above electrochemical performance of C-NVP and CDC against Na metal foil, the optimized mass ratio between C-NVP and CDC was 1:3. The constructed NHC was tested between 0 and 3 V to evaluate its electrochemical performance. The obtained cyclic voltammetry (Figure SS10, Supporting Information) curve is an asymmetrical one rather than the ideal rectangular curve obtained for symmetrical capacitors. This confirms the presence of two charge storage mechanisms in the NHC, one based on the intercalation/deintercalation of Na ions in the C-NVP and other based on non-faradaic surface charge storage in the CDC.[30,56,57] Although the shape of the CV curve deviates from a regular rectangular one, it retains its shapes with increasing scan rate. This shows that the hybrid capacitor would exhibit high stability in the

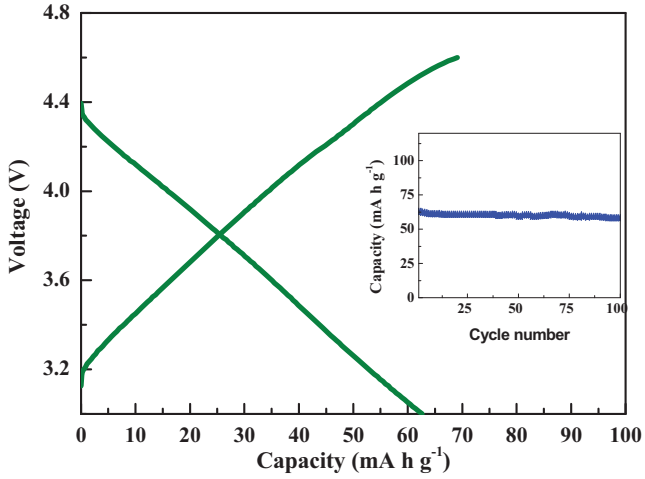

Figure 5. Charge/discharge profile and cyclic stability of CDC, tested between 3 and 4.6 V versus Na at 400 mA h g^{-1}.

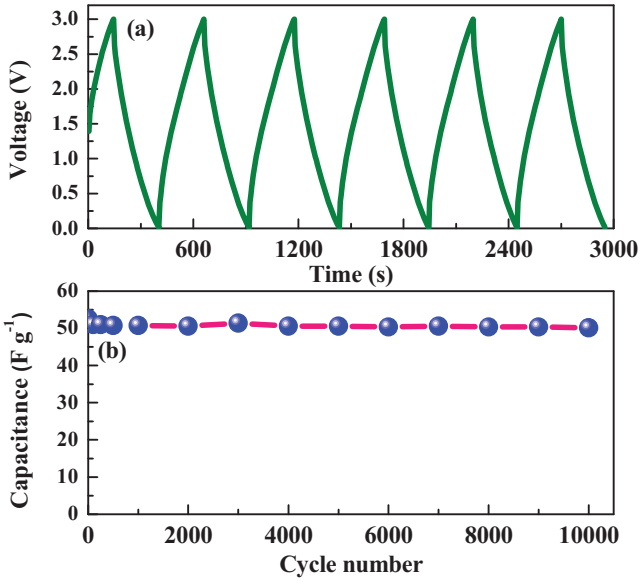

Figure 6. a) Charge/discharge curves and b) cyclic stability of NHC at 1.1 mA cm^{-2} between 0 and 3 V.

nonaqueous electrolyte, even at high current rates. However, the capacitance of the NHC decreases with increasing scan rate because the diffusion of Na^+ ions is restricted to just the surface of the electrode material. The bulk of the material is not utilized because Na^+ ions cannot diffuse into it owing to their quick diffusion rate at higher scan rates.[27,55]

The galvanostatic behavior of the NHC was tested between 0 and 3 V at different current densities. Figure SS 11 (Supporting Information) shows the charge–discharge profile of NHC at different current densities. The obtained curves were not ideal triangles, as with EDLC capacitors. These irregular triangles have a plateau around 1.5 V along with a sloping line and this again confirms the operation of two different charge storage mechanisms in the NHC.[26,56–58] The plateau is based on the faradaic intercalation/deintercalation of Na^+ ions and the sloping line is based on simultaneous nonfaradaic surface adsorption/desorption, and thus the NHC possess both battery and supercapacitor behavior. The reduction in size of plateau in discharge curve with increasing current density is mainly due to the decline in number of sodium ions intercalated into the C-NVP. At increased current rate, sodium ions intercalate only into the surface as ionic diffusion is greatly reduced at this condition and it is in correlation with results from cyclic voltammetry.[27,55,56] Even at this condition this novel NHC performs well as a large number of pores available on the surface of C-NVP particles provides the way for more number of sodium ions to intercalate into C-NVP easily. The proposed reaction mechanism is as follows

$$Na_3V_2^{3+}(PO_4)_3 + xe^- \leftrightarrow Na_{3+x}V_2^{2+}(PO_4)_3$$
$$CDC \leftrightarrow CDC\ +//xClO_4^-\ xe^-$$
$$(//-\text{double layer})$$

When the NHC is charged initially, Na^+ ions intercalate into the C-NVP from the electrolyte, which causes a charge imbalance in the electrolyte. To compensate this, ClO_4^{-1} anions are adsorbed over the CDC surface and form a double layer. During discharge, ClO_4 is desorbed from the CDC surface into the electrolyte and Na^+ ions are deintercalated back to the electrolyte. Intercalation and deintercalation of Na^+ ions and ClO_4 anion adsorption/desorption are highly reversible processes. This combined mechanism of nonfaradaic double layer formation and faradaic intercalation/deintercalation contributes to the power density and energy density, respectively, of NHC capacitors.[27,30,55–59] The schematic diagram on working mechanism of NHC has been presented in Figure SS 12 in the Supporting Information.

The discharge specific capacitances of NHC were 105, 96, 85, 80, 61, and 53 F g^{-1} at current densities of 0.12, 0.24, 0.35, 0.6, 0.8, and 1 mA cm^{-2}, respectively. The results are in good correlation with the CV profile, i.e., with increasing current density, the discharge time decreases and retains a low discharge specific capacitance. This indicates that only the surface of the electrode material takes part in the reaction and not the bulk material.[55,60] To determine the long-term performance of NHC, it was tested at a current density of 1.1 mA cm^{-2} and the results are presented in **Figure 6**a,b. The NHC cell delivered a specific capacity of 52.58 F g^{-1} in the first cycle and 50.13 F g^{-1} at the 10 000th cycle, thus retaining more than 95% of the initial capacitance. The first few cycles are utilized in structural stabilization; the cells deliver 51 F g^{-1} at the 100th cycle and exhibit almost no capacitance fading thereafter.

These results reveal that the constructed NHC delivers high discharge capacitance at high current and that it retains extraordinary stability, as shown in Figure 6b. To the best of our knowledge, this is the first intercalation-based sodium electrode with highest stability that has been reported for NHC application. It also outperforms many lithium intercalation electrodes in terms of stability and performance, which is compared in **Table 1**. The practical applicability of NHC is shown by the Ragone plot in **Figure 7**b. A high energy density of 118 Wh kg^{-1} was achieved at a specific power of 95 W kg^{-1}. It also achieved a high specific power of 850 W kg^{-1} and retained an energy density of 60 Wh kg^{-1}. This clearly shows that this new novel NHC system outperforms many

Table 1. Comparison of energy density, power density, and stability of various systems

System	Energy density [Wh kg^{-1}]	Power density [W kg^{-1}]	Stability
Our work	60	850	95% after 10 000 cycles
AC/$LiCoO_2$[61]	32	100	40% after 3000 cycles
AC/Li_2MnSiO_4[62]	37	1400	85% after 1000 cycles
AC/$LiMn_2O_4$[61]	38	100	98% after 3000 cycles
AC/$Li_4Ti_5O_{12}$[63]	10	1000	84% after 9000 cycles
AC/$LiCoPO_4$[27]	11	1607	67% after 1000 cycles
AC/Li_2CoPO_4F[27]	16	1607	92% after 30 000 cycles
AC/TiO_2-B[64]	18	235	73% after 1200 cycles
AC/$LiCo_{1/3}Ni_{1/3}Mn_{1/3}O_2$[61]	42	100	90% after 500 Cycles
AC/$LiMn_{1.5}Ni_{0.5}O_4$[26]	56	130	81% after 3000 cycles
AC/$LiTi_2(PO_4)_3$[65]	14	180	48% after 1000 cycles
AC/$Li_3V_2(PO_4)_3$[66]	27	255	66% after 1000 cycles
AC/$NaMn_{1/3}Ni_{1/3}Co_{1/3}PO_4$[67]	15	400	95% after 1000 cycles
AC/Na-TNT[68]	34	889	98% after 1000 cycles
AC/V_2O_5-CNT[69]	38	140	80% after 1000 cycles
NVP/carbon composite[44]	26	290	65% after 10 000 cycles

Li-ion hybrid capacitors. Also, the novel bio-inspired system possesses the highest stability ever reported.[26,61–68] The performance of various lithium-based intercalation materials is presented in Table 1. It is clearly seen that this novel CDC//C-NVP system outperforms most of the attractive lithium intercalation materials such as $LiCoO_2$,[61] $Li_3V_2(PO_4)_3$,[65] $LiMn_{1.5},Ni_{0.5}O_4$,[26] Li_2MnSiO_4,[62] $LiCo_{1/3}Mn_{1/3}Ni_{1/3}O_2$,[61] $Li_4Ti_5O_{12}$,[63] and pseudocapacitance materials such as TiO_2-B.[69] Also, this novel system is superior to all currently reported sodium ion hybrid capacitors, as well as NVP/carbon symmetric capacitors[43] in terms of power density, energy density, and stability. To verify the reason behind this excellent performance, a Nyquist plot was recorded for the constructed NHC in its initial and 10 000th cycles, and the results are presented in **Figure 8**. As anticipated, the NHC exhibits a semicircle due to the charge transfer reaction in the high-frequency region and also an incline in the low-frequency region as this is a diffusion-controlled process.[56,58] Although there is an increase in electrolyte resistance after the 10 000th cycle due to unwanted side reactions between the electrode and electrolyte at the initial stage, the charge transfer resistance did not seem to increase, demonstrating a slight decrease in the charge transfer resistance, which means that the electrode surface was fully available for reversible ionic intercalation.

The following are the main reasons for the excellent performance of the NHC system: (i) The structurally stable C-NVP retained its polyanion framework structure, even at high current charge/discharge conditions. Also, the enhanced cyclability was synergistically improved by the uniform nanocarbon coating, which not only increased the current flow on the particle surface but also helped in retaining the polyanion framework by preventing side reactions with the electrolyte. (ii) The $Na_3V_2(PO_4)_3$–NASCION material had a high Na^+ diffusion coefficient. Further, its electrochemical reaction kinetics were significantly improved by the presence of smaller, highly crystalline mesopores, along with the nanocarbon coating and carbon bridge. This significantly increased the electronic conductivity and provided an easier and shorter path for electronic movement; it also reduced the ion transport resistance. (iii) The charge transfer resistance did not increase with increased cycling. Instead, there was slight reduction in charge transfer resistance, which means that the surface was still active and performed well. Similarly, sodium ion diffusion was easy, penetrating deeply into the surface. (iv) The highly porous nature of C-NVP and CDC also played a vital role in enhancing the capacitance behavior of the NHC cell. Mesopores in NVP and

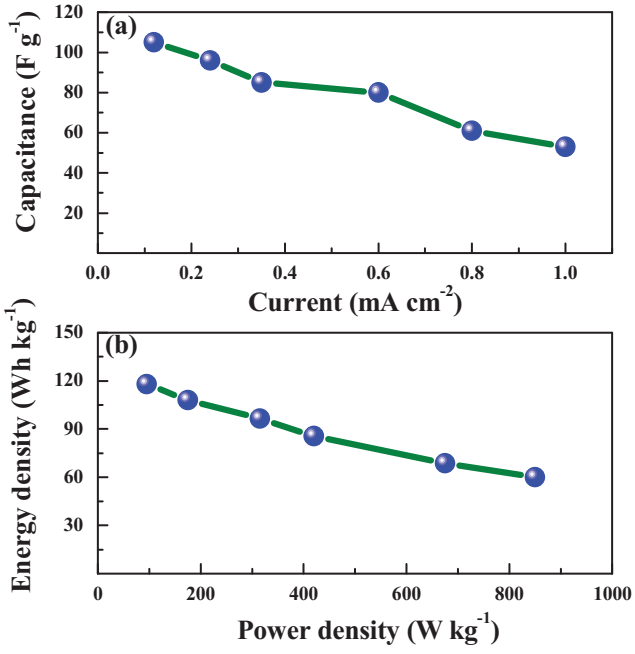

Figure 7. a) Rate performance of NHC and b) Ragone plot for NHC at different current densities.

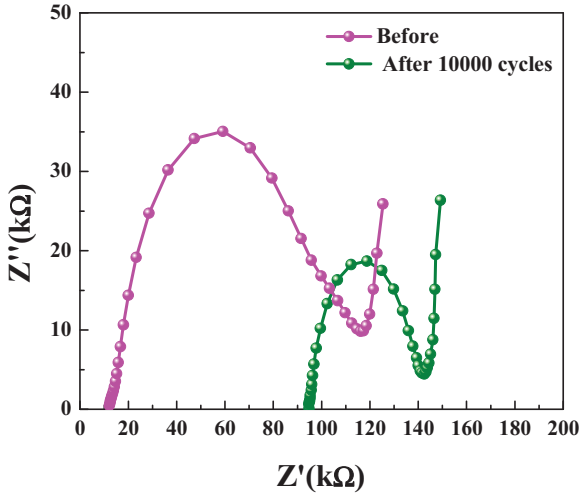

Figure 8. Nyquist plots of CDC/C-NVP NHC between 200 and 100 MHz before and after 10 000 cycles at a current density of 1.1 mA cm^{-2}.

the combination of micro and mesopores in CDC remarkably increased the electrode–electrolyte interface by storing the electrolyte, which significantly boosted the surface reaction. (v) Moreover, electrodes with highly porous nature held more electrolyte within their structures and provided a flexible structure against the mechanical stress formed during the cycling process at high current rates. It was expected that these unique properties of the composite materials would enable the achievement of excellent cycling performance, even with high charge–discharge cycling processes. (vi) The appropriate kinetic and mass balance, along with low internal resistance, made this NHC highly stable. They also provided high energy and high power density. These results clearly demonstrated that a 3 V high-performance NHC could be fabricated using C-NVP and CDC electrodes in an organic electrolyte for future EVs application.

4. Conclusion

We successfully constructed a novel bio-inspired sodium ion hybrid capacitor using superionic conductor $Na_3V_2(PO_4)_3$ and a cinnamon-derived highly porous, eco-friendly, activated carbon in an organic electrolyte. This novel system delivered a superior energy density of 118 Wh kg^{-1} and a power density of 850 W kg^{-1}, along with excellent stability. These values are the highest ever reported for sodium ion-based intercalation compounds, and they are even superior in terms of performance to many Li ion-based intercalation and other insertion compounds. This could thus be an alternative to current Li ion-based energy storage systems. With its superior and remarkable performance, the proposed system is a candidate for next-generation EVs and HEVs. With more research and optimization in modern engineering, this could be made possible in future.

5. Experimental Section

Carbon-coated $Na_3V_2(PO_4)_3$ was synthesized by the sol–gel technique using Na_2CO_3, V_2O_5, and $NH_4H_2PO_4$ as precursors. Oxalic acid was used both as a reducing agent and a chelating agent. Ethylene glycol was used as the carbon source, which is also a reducing agent. Oxalic acid and ethylene glycol form a porous uniform carbon network around the NVP particle and inhibit its particle growth at high temperature, thus improving its electronic conductivity. Stoichiometric amount of V_2O_5 was initially dissolved in oxalic acid at 90 °C in water and then the other precursors were added. The solution formed at 120 °C was subjected to two-step heat treatment at 350 °C for 3 h and 700 °C for 8 h in an Ar/H_2 atmosphere.

To synthesize highly porous carbon, cinnamon sticks obtained from a local supermarket were used as the starting material. The cinnamon sticks were broken into smaller pieces, washed with water, and dried at 80 °C for two days. Then, sticks were carbonized at 300 °C for 2 h and then ground well and treated with KOH at a weight ratio of 1:5. The mixture was pyrolyzed at 650 °C for 1.5 h under argon atmosphere. The product was washed with 0.1 M HCl and distilled water several times to remove the residual K^+ ions. The washed product was then vacuum dried overnight and used for constructing a hybrid capacitor.

Supporting Information

Supporting Information is available from the Wiley Online Library or from the author.

Acknowledgements

R.T. and Dr. K.K. contributed equally to this work. This work was supported by Samsung Research Funding Center of Samsung Electronics under Project Number SRFC-TA1403-03.

Received: November 5, 2015
Revised: December 12, 2015
Published online: January 19, 2016

[1] N. Yabuuchi, M. Kajiyama, J. Iwatate, H. Nishikawa, S. Hitomi, R. Okuyama, R. Usui, Y. Yamada, S. Komaba, *Nat. Mater.* **2012**, *11*, 512.
[2] R. Berthelot, D. Carlier, C. Delmas, *Nat. Mater.* **2011**, *10*, 74.
[3] J. M. Tarascon, M. Armand, *Nature* **2001**, *414*, 359.
[4] M. Armand, J. M. Tarascon, *Nature* **2008**, *451*, 652.
[5] M. S. Whittingham, *Chem. Rev.* **2004**, *104*, 4271.
[6] F. Y. Cheng, J. Liang, Z. L. Tao, J. Chen, *Adv. Mater.* **2011**, *23*, 1695.
[7] V. Etacheri, R. Marom, R. Elazari, G. Salitra, D. Aurbach, *Energy Environ. Sci.* **2011**, *4*, 3243.
[8] C. D. Wessells, R. A. Huggins, Y. Cui, *Nat. Commun.* **2011**, *2*, 550.
[9] H. Pan, Y. S. Hu, L. Chen, *Energy Environ. Sci.* **2013**, *6*, 2338.
[10] S. W. Kim, D. H. Seo, X. Ma, G. Ceder, K. Kang, *Adv. Energy Mater.* **2012**, *2*, 710.
[11] B. L. Ellis, W. R. M. Makahnouk, W. N. Rowan-Weetaluktuk, D. H. Ryan, L. F. Nazar, *Chem. Mater.* **2009**, *22*, 1059.
[12] D. Aurbach, Y. Gofer, Z. Lu, A. Schechter, O. Chusid, H. Gizbar, Y. Cohen, V. Ashkenazi, M. Moshkovich, R. Turgeman, E. Levi, *J. Power Sources* **2001**, *97–8*, 28.
[13] M. D. Slater, D. Kim, E. Lee, C. S. Johnson, *Adv. Funct. Mater.* **2013**, *23*, 947.
[14] P. Senguttuvan, G. Rousse, V. Seznec, J. M. Tarascon, M. R. Palacin, *Chem. Mater.* **2011**, *23*, 4109.
[15] H. Yu, S. Guo, Y. Zhu, M. Ishida, H. Zhou, *Chem. Commun.* **2014**, *50*, 457.
[16] W. K. Pang, S. Kalluri, V. K. Peterson, N. Sharma, J. Kimpton, B. Johannessen, H. K. Liu, S. X. Dou, Z. Guo, *Chem. Mater.* **2015**, *27*, 3150.
[17] R. Berthelot, D. Carlier, C. Delmas, *Nat. Mater.* **2011**, *10*, 74–U73–.
[18] S. M. Oh, S. T. Myung, C. S. Yoon, J. Lu, J. Hassoun, B. Scrosati, K. Amine, Y. K. Sun, *Nano Lett.* **2014**, *14*, 1620.
[19] Z. Jian, W. Han, X. Lu, H. Yang, Y.-S. Hu, J. Zhou, Z. Zhou, J. Li, W. Chen, D. Chen, L. Chen, *Adv. Energy Mater.* **2013**, *3*, 156.
[20] K. Saravanan, C. W. Mason, A. Rudola, K. H. Wong, P. Balaya, *Adv. Energy Mater.* **2013**, *3*, 444.
[21] M. Guignard, C. Didier, J. Darriet, P. Bordet, E. Elkaïm, C. Delmas, *Nat. Mater.* **2013**, *12*, 74.
[22] K. Chihara, A. Kitajou, I. D. Gocheva, S. Okada, J. Yamaki, *J. Power Sources* **2013**, *227*, 80.
[23] K. Sakaushi, E. Hosono, G. Nickerl, T. Gemming, H. Zhou, S. Kaskel, J. Eckert, *Nat. Commun.* **2013**, *4*, 1485.
[24] M. Sathiya, K. Hemalatha, K. Ramesha, J. M. Tarascon, A. S. Prakash, *Chem. Mater.* **2012**, *24*, 1846.
[25] Y. Jiang, Z. Yang, W. Li, L. Zeng, F. Pan, M. Wang, X. Wei, G. Hu, L. Gu, Y. Yu, *Adv. Energy Mater.* **2015**, *5*, 1402104.
[26] N. Arun, A. Jain, V. Aravindan, S. Jayaraman, W. C. Ling, M. P. Srinivasan, S. Madhavi, *Nano Energy* **2015**, *12*, 69.
[27] K. Karthikeyan, S. Amaresh, K. J. Kim, S. H. Kim, K. Y. Chung, B. W. Cho, Y. S. Lee, *Nanoscale* **2013**, *5*, 5958.
[28] G. G. Amatucci, F. Badway, A. Du Pasquier, T. Zheng, *J. Electrochem. Soc.* **2001**, *148*, A930.
[29] V. Aravindan, J. Gnanaraj, Y. S. Lee, S. Madhavi, *Chem. Rev.* **2014**, *114*, 11619.

[30] E. Lim, H. Kim, C. Jo, J. Chun, K. Ku, S. Kim, H. Ik Lee, I. S. Nam, S. Yoon, K. Kang, J. Lee, *ACS Nano* **2014**, *8*, 8968.
[31] Y. Wang, Z. Hong, M. Wei, Y. Xia, *Adv. Funct. Mater.* **2012**, *22*, 5185.
[32] S. Y. Lim, H Kim, R. A. Shakoor, Y. Jung, J. W. Choi, *J. Electrochem. Soc.* **2012**, *159*, A1393.
[33] Q. An, F. Xiong, Q. Wei, J. Sheng, L. He, D. Ma, Y. Yao, L. Mai, *Adv. Energy Mater.* **2015**, *5*, 1401963.
[34] Y. H. Jung, C. H. Lim, D. K. Kim, *J. Mater. Chem. A* **2013**, *1*, 11350.
[35] Y. Fang, L. Xiao, X. Ai, Y. Cao, H. Yang, *Adv. Mater.* **2015**, *27*, 5895.
[36] X. Rui, W. Sun, C. Wu, Y. Yu, Q. Yan, *Adv. Mater.* **2015**, *27*, 6670
[37] S. Li, Y. Dong, Lin Xu, X. Xu, Liang He, Liqiang Mai, *Adv. Mater.* **2014**, *26*, 3545.
[38] S. J. Lim, D. W. Han, D. H. Nam, K. S. Hong, J. Y. Eom, W. H. Ryu, H. S. Kwon, *J. Mater. Chem. A* **2014**, *2*, 19623.
[39] H. Li, X. Yu, Y. Bai, F. Wu, C. Wu, L. Y. Liu, X. Q. Yang, *J. Mater. Chem. A* **2015**, *3*, 9578.
[40] C. Zhu, K. Song, P. A. Van Aken, J. Maier, Y. Yu, *Nano Lett.* **2014**, *14*, 2175.
[41] E. Frackowiak, F. Beguin, *Carbon* **2001**, *39*, 937.
[42] L. Wei, G. Yushin, *Nano Energy* **2012**, *1*, 552.
[43] M. Biswal, A. Banerjee, M. Deo, S. Ogale, *Energy Environ. Sci.* **2013**, *6*, 1249.
[44] Z. Jian, V. Raju, Z. Li, Z. Xing, Y. S. Hu, X. Ji, *Adv. Funct. Mater.* **2015**, *25*, 5778.
[45] Z. Jian, L. Zhao, H. Pan, Y. S. Hu, H. Li, W. Chen, L. Chen, *Electrochem. Commun.* **2012**, *14*, 86.
[46] A. C. Ferrari, J. C. Meyer, V. Scardaci, C. Casiraghi, M. Lazzeri, F. Mauri, S. Piscanec, D. Jiang, K. S. Novoselov, S. Roth, A. K. Geim, *Phys. Rev. Lett.* **2006**, *97*, 187401.
[47] W. Zhang, Y. Liu, C. Chen, Z. Li, Y. Huang, X. Hu, *Small* **2015**, *27*, 3822.
[48] J. Mendialdua, R. Casanova, Y. Barbaux, *J. Electron Spectrosc.* **1995**, *71*, 249.
[49] N. Kumar, R. Radhika, A. T. Kozakov, K. J. Sankaran, S. Dash, A. K. Tyagi, N. H. Tai, I. N. Lin, *J. Phys. D* **2013**, *46*, 275501.
[50] Y. J. Kim, B.-J. Lee, H. Suezaki, T. Chino, Y. Abe, T. Yanagiura, K. C. Park, M. Endo, *Carbon* **2006**, *44*, 1592.
[51] A. C. Ferrari, J. Robertson, *Phys. Rev. B* **2000**, *61*, 14095.
[52] D. W. Wang, A. Du, E. Taran, G. Q. Lu, I. R. Gentle, *J. Mater. Chem.* **2012**, *22*, 21085.
[53] D. Wang, N. Chen, M. Li, C. Wang, H. Ehrenberg, X. Bie, Y. Wei, G. Chena, F. Du, *J. Mater. Chem. A* **2015**, *3*, 8636.
[54] Z. Jian, Y. Sunb, X. Ji, *Chem. Commun.* **2015**, *51*, 6381.
[55] K. Karthikeyan, V. Aravindan, S. B. Lee, I. C. Jang, H. H. Lim, G. J. Park, M. Yoshio, Y. S. Lee, *J. Alloys Compd.* **2010**, *504*, 224.
[56] K. Karthikeyan, S. Amaresh, V. Aravindan, H. Kim, K. S. Kang, Y. S. Lee, *J. Mater. Chem. A* **2013**, *1*, 707.
[57] H. Kim, M. Y. Cho, M. H. Kim, K. Y. Park, H. Gwon, Y. S. Lee, K. C. Roh, K. Kang, *Adv. Energy Mater.* **2013**, *3*, 1500.
[58] K. Karthikeyan, S. Amaresh, S. N. Lee, J. Y. An, Y. S. Lee, *ChemSusChem* **2014**, *7*, 2310.
[59] K. Karthikeyan, S. Amaresh, S. N. Lee, V. Aravindan, Y. S. Lee, *Chem.- Asian J.* **2013**, *9*, 852.
[60] N. Yu, L. Gao, *Electrochem. Commun.* **2009**, *11*, 220.
[61] Y. Wang, J. Luo, C. Wang, Y. Xia, *J. Electrochem. Soc.* **2006**, *153*, A1425.
[62] K. Karthikeyan, V. Aravindan, S. B. Lee, I. C. Jang, H. H. Lim, G. J. Park, M. Yoshio, Y. S. Lee, *J. Power Sources* **2010**, *195*, 3761.
[63] I. Plitz, A. D. Pasquier, F. Badway, J. Gural, N. Pereira, A. Gmitter, G. G. Amatucci, *Appl. Phys. A* **2006**, *82*, 615.
[64] V. Aravindan, W. Chuiling, M. V. Reddy, G. V. S. Rao, B. V. R. Chowdari, S. Madhavi, *Phys. Chem. Chem. Phys.* **2012**, *14*, 5808.
[65] R. Satish, V. Aravindan, W. C. Ling, S. Madhavi, *J. Power Sources* **2015**, *281*, 310.
[66] M. Minakshi, D. Meyrick, D. Appadoo, *Energy Fuels* **2013**, *27*, 3516.
[67] J. Yin, L. Qi, H. Wang, *ACS Appl. Mater. Interfaces* **2012**, *4*, 2762.
[68] Z. Chen, V. Augustyn, X. Jia, Q. Xiao, B. Dunn, Y. Lu, *ACS Nano* **2012**, *6*, 4319.
[69] V. Aravindan, N. Shubha, W. Chui Ling, S. Madhavi, *J. Mater. Chem. A* **2013**, *1*, 6145.

